Climatology of Aerosol Optical Properties at Storm Peak Laboratory

Crystal M. Japngie-Green[1], Elisabeth Andrews[3,4], Ian B. McCubbin[2], John A. Ogren[3,4], and *Anna G. Hallar[1,2]

[1]Dept. Atmospheric Sciences, University of Utah, Salt Lake City, UT, USA
[2]Storm Peak Laboratory, Desert Research Institute, Steamboat Springs, CO, USA
[3]NOAA, Earth System Research Laboratory, Boulder, CO, USA
[4]Cooperative Institute for Research in Environmental Sciences, University of Colorado, Boulder, CO, USA

Abstract

Aerosols create large uncertainty in the planetary energy balance due to both direct and indirect radiative forcing. Understanding aerosol seasonal patterns is essential for accurate climate change prediction. Mountain regions are often difficult for climate models to resolve. Therefore, long term observations collected at high elevations are particularly useful. In-situ surface aerosol optical measurements were analyzed for the years 2011 – 2016 at a mountain site located in western Colorado and tied to potential sources based on relationships among the aerosol properties.

Peak scattering and absorption coefficients were observed during the summer months, suggesting greater aerosol loading (likely due to wildfires), and were lowest during the winter months indicating cleaner conditions (due to less boundary layer influence). The scattering Ångström exponent, a property that provides information about size distributions, revealed coarse-mode particles during the spring, which is consistent with dust aerosols. During the summer months the scattering Ångström exponent revealed size distributions composed of mostly fine-mode particles. This observed increase in fine particles points to the presence of

* Correspondence to: A.G. Hallar
Email: gannet.hallar@utah.edu
Fax: 801-585-3681
Telephone: 801-587-7238

combustion aerosols, likely attributable to wildfires during the dry season (Hallar, 2015). The absorption Ångström exponent was lowest (close to one) during the summer which is consistent with the presence of combustion aerosols and was slightly higher (~1.3) during the spring season. Schmeisser et al. (2017) suggests that, for in-situ aerosol, absorption Angstrom exponents larger than 1.5 may be indicative of dust if they are associated with low (< 1.3) scattering Angstrom exponents. The increase in combustion aerosols during the summer accompanied by high values for single scattering albedo suggests that these aerosols have undergone processing in the atmosphere before reaching Storm Peak Laboratory. These results are important for improving visibility and predicting future aerosol concentrations in the Western U.S.

1 INTRODUCTION

Atmospheric aerosols change rapidly over short time intervals making future concentrations difficult to predict (Laj et al, 2009). Establishing aerosol climatology is important for identifying aerosol sources, distributions and transport (Hand et al., 2017; Yu et al., 2009). By revealing seasonal aerosol patterns of a region, improvements can be made to climate models (Chung et al., 2005) and visibility by identifying aerosol sources (Hirdman et al., 2010). There is large disagreement among climate models related to aerosol spatial distributions and the direct and indirect radiative forcing effects of these aerosols (Reddington et al., 2017).

Aerosols absorb and scatter radiation, and thus have a direct effect on the planetary energy balance. These effects can be quantified by calculating direct radiative forcing from measured aerosol optical properties. Direct aerosol radiative forcing is dependent upon particle composition, size and concentration (Haywood and Boucher, 2000). The most current estimate from the Intergovernmental Panel on Climate Change of direct aerosol radiative forcing is -0.35 $\pm$ 0.5 W/m^2 (Stocker et al., 2013). The large uncertainty associated with this value is a

consequence of rapidly changing aerosol distributions with respect to time and location (Stocker et al., 2013), model uncertainties (Reddington et al., 2017), and varied aerosol composition (Jacobson, 2001).

Aerosols also influence the radiation balance by indirect mechanisms. Due to their role as potential cloud condensation nuclei (CCN), aerosols can change the energy balance by altering cloud properties. When CCN concentrations are high, clouds will be composed of more droplets of smaller diameter and thus different optical properties (Twomey, 1977). Clouds composed of smaller droplets can persist longer due to delayed precipitation resulting in further changes to the radiation balance (Albrecht, 1989).

Feedbacks that influence future aerosol climatology are another important consideration for numerical model accuracy. For example, wildfires are a common source of atmospheric aerosols during the summer months and are expected to increase as the climate warms (Spracklen et al., 2009). Increased aerosol loading leads to diminished incoming solar radiation at the surface due to light extinction (Charlson et al., 1992). Decreased solar radiation has been linked to milder summer monsoons in the southwestern U.S. (Diffenbaugh et al., 2006). A strong correlation between drought and wildfire has also been observed (Westerling et al., 2006), ultimately creating a positive feedback for aerosol loading and additional cooling of the climate system. Using numerical models, Spracklen et al. (2009) projected a 40% increase in organic carbon due to increased wildfire activity by the year 2050. Hallar et al. (2017) have estimated this value to be lower, at 24% for the Colorado Rockies and 36% for the Wasatch and Uintah Mountains, an important consideration for numerical climate models since aerosols moderate warming. The net effect of these mechanisms is unclear due to competing feedbacks that are not well understood or quantified.

Previous studies and climate models have relied heavily on aerosol optical depth (AOD) in order to observe aerosol loading and transport. AOD is an integrated measurement of aerosols throughout the entire atmospheric column that is measured using satellite or ground-based radiometers. Satellite measurements are particularly valuable because they can gather aerosol data over large areas (Wang et al., 2012). While useful, these measurements lack information regarding the vertical distribution of aerosols within the column. The vertical distribution has an effect on radiative forcing (Sanroma et al., 2010) and can also provide information about aerosol transport and sources. For example, greater AODs have been observed during the spring with the transport of Asian dust to North America by extratropical cyclones (Yu et al., 2008). Hallar et al. (2015) observed that, at their mountain site in Colorado, in-situ measurements made at the surface did not spike in the spring with AOD measurements, suggesting the aerosols contributing to the seasonal increase in AOD were located above the surface.

Surface in-situ measurements can provide additional aerosol information using different methodologies than those used to find AOD. Unlike remote sensing measurements, for in-situ measurements the air is sampled within instruments to obtain aerosol absorption and scattering. This approach allows continuous data to be obtained at the surface at a specific location regardless of atmospheric conditions (e.g., clouds, nighttime, etc.). For some aerosol properties, such as absorption and single scattering albedo, remote sensing techniques can have high uncertainty, emphasizing the importance of in-situ measurements (Dubovik, 2000). Combining remote sensing with in-situ measurements provides more comprehensive information for improving direct radiative forcing estimates (Andrews et al., 2004; Yu et al., 2009).

While global values of radiative forcing have large uncertainty, regional estimates are even more variable (Yu et al., 2009). Gathering long term in-situ data from various sites is one

way to reduce this uncertainty (Andrews et al., 2011; Pandolfi et al., 2018). Mountain regions create unique difficulties for climate models due to complex terrain and insufficient model resolution (Giorgi, 2005). Therefore, data collected at high elevations will be especially valuable for improving climate models, particularly as the spatial resolution of the models improve.

In the following, in-situ aerosol optical property data collected from 2011 – 2016 at a high elevation site in the western U.S. are analyzed to identify seasonal aerosol trends. Scattering and absorption coefficients are used to calculate a variety of aerosol optical properties that can help to establish the aerosol climatology of the region and illuminate the possible sources of these aerosols.

2 METHODOLOGY

2.1 LOCATION

Storm Peak Laboratory (SPL) is a mountain-top site (3220 m) located in western Colorado (40.455° N, 106.745°). Due to its remote location, SPL has little influence from traffic or industry of nearby cities (Hallar et al., 2016) and has been used for aerosol research since the 1990s. All data for this project was collected at SPL and went through a quality assurance process to remove spikes due to local contamination (e.g., ski area vehicles) as well as periods when the instruments were not working or being maintained. The edited data was submitted to the EBAS Level 2 data archive (http://ebas.nilu.no). Measurements were taken in one-minute intervals, but Level 2 data are reported as hourly averages. The Level 2 data are also reported at standard temperature (273.15 K) and pressure (1013.25 hPa) and the appropriate instrument corrections are applied as described below.

2.2 INSTRUMENTATION

The scattering data were collected using a TSI 3563 nephelometer that measures the scattering coefficient σ_{sp} at 3 wavelengths (λ) (450nm, 550nm, and 700nm). The nephelometer data were corrected for instrument angular truncation and light source non-idealities (Anderson and Ogren, 1998). A particle soot absorption photometer (PSAP) was used to measure the absorption coefficient σ_{ap} at slightly different visible wavelengths (467nm, 530nm, and 660nm). Data from the PSAP was replaced in 2013 by data from a similar instrument known as a continuous light absorption photometer (CLAP, wavelengths: 467nm, 528nm and 652nm). This instrument measures absorption in the same manner as the PSAP, but contains 8 filter spots (compared to one filter spot for the PSAP) that it rotates through before filter replacement is required (Ogren et al., 2017). This is advantageous because SPL is a remote site with infrequent technician visits. PSAP and CLAP data were corrected using the schemes in Bond et al. (1999) to account for scattering artifacts, spot size and flow and Ogren (2010) to extend the Bond corrections for all three wavelengths. Data where the filter transmittance was less than 0.5 were automatically marked as invalid during the QC process because of limitations of the Bond correction.

A switched impactor system separates aerosols into particulate matter less than 10 μm (PM_{10}) and particulate matter less than 1 μm (PM_1) before measurements are made by the nephelometer and PSAP/CLAP. For measurements of this type, the sample air is often dried to achieve a relative humidity of 40 percent or less to avoid the confounding effects of water on aerosol properties. Because SPL is located in an arid region and the measurements are made within a heated building, relative humidity values above 40 percent are rare (Hallar et al., 2015), eliminating the need for this step.

2.3 CALCULATIONS

The measured scattering and absorption coefficients offer information about aerosol loading at the surface. These values can also be used to calculate various intensive aerosol optical properties (intensive properties are independent of the amount of aerosol loading). The scattering Ångström exponent and absorption Ångström exponent can be calculated using measurements made at two wavelengths ($\alpha_x = - \log(\sigma_{xp}(\lambda_1)/ \sigma_{xp}(\lambda_2)/\log(\lambda_1/\lambda_2))$) where $\sigma_{xp}(\lambda_i)$ is the scattering (s) (or absorption (a)) at wavelength i. The scattering Ångström exponent (α_s) can be used as an indicator of particle size, with low values corresponding to aerosols with greater diameter and higher values indicating small diameter particles. Clarke and Kapustin (2010) experimentally obtained a threshold ($\alpha_s = 1.3$) for the scattering Ångström exponent (450 nm/700 nm) that differentiates between fine-mode aerosols ($\alpha_s > 1.3$) and coarse-mode aerosols ($\alpha_s < 1.3$). The absorption Ångström exponent (α_a) can provide information about the composition of aerosols (e.g., Bergstrom et al., 2002,; 2007). Black carbon has a theoretical value of $\alpha_a = 1$, while dust aerosol α_a tends to be larger than 2 and there is no clear consensus on typical values for biomass burning (Table 1 in Schmeisser et al., 2017 and references therein). The single-scattering albedo (SSA) is the ratio of scattering coefficient to the extinction coefficient (the sum of absorption and scattering). SSA is high (close to 1) for aerosols that readily scatter light and lower for aerosols that strongly absorb light (black carbon has SSA~0.3), providing additional information about aerosol type.

5 RESULTS AND DISCUSSION

Fig. 1(a) shows the monthly means for PM_1 and PM_{10} of scattering coefficients at each wavelength (450nm, 550nm and 700nm). In all cases, the highest values are found during the summer months, with the peak in August. The lowest values occur during the winter months, when air is cleaner due to SPL being less influenced by the atmospheric boundary layer, which is

generally the case for mountain sites (Raatikainen et al., 2014). The rate of change from spring to summer is more gradual than from summer to fall. It is probable that the spike in aerosol scattering during the summer is due to biomass burning during peak wildfire season (Hallar et al., 2015).

Monthly averages for absorption coefficients are shown in Fig. 1(b). The PSAP or CLAP absorption data were adjusted to 450nm, 550nm and 700nm using the absorption Angstrom exponent. This was done to accommodate calculation of SSA which requires both absorption and scattering coefficients at the same wavelength. The absorption data follows a similar pattern to the scattering data with the highest monthly values found during the summer season and lowest values during the winter months. As with scattering, the slope of the curve from spring to summer is not as steep as the slope from summer to fall.

While aerosol loading is an important factor for radiative forcing, information about the aerosol size distribution and composition can aid in attributing aerosol forcing to different sources. For example, natural particles such as dust tend to dominate the coarse mode (diameter > 1μm), while anthropogenic and combustion aerosol are more dominant in the fine mode (diameter < 1 μm). When calculating the scattering Ångström exponent an additional constraint on the scattering data was applied. Similar to Andrews et al. (2011) scattering values less than 0.5 Mm^{-1} were omitted when calculating the scattering Ångström exponent with the purpose of minimizing noise that can occur when taking the ratio of two small numbers. This method eliminated 7.45 % of the scattering data for PM_1 and 6.69% of the data for PM_{10}. Fig. 2(a) shows the monthly averaged scattering Ångström exponent for PM_1 and PM_{10}. The scattering Ångström exponent is lowest during the spring months, particularly in March when the mean value drops to 1.3, indicating the presence of large particles at the surface – these particles are likely dust

(Hallar et al., 2015), although whether they are from regional sources or due to long range transport is unclear. During the summer months, the scattering Ångström exponent is at its highest (~2 for PM_{10}), corresponding to a greater contribution from small particles. This is likely due to increased combustion aerosols during peak wildfire activity (Hallar et al., 2015).

The monthly averaged absorption Ångström exponent is presented in Fig. 2(b). The α_a at SPL exhibits less seasonal variation than other aerosol optical properties ranging only between 1 and 1.3 throughout the year. The lowest α_a (near 1) occurred during the summer months. The highest values for α_a occurred during spring season. Some winter months also exhibit higher values of α_a; however, SPL is an extremely remote site with the cleanest conditions occurring during the winter months which can lead to noise in the α calculation. The springtime values for α_a found at SPL are lower than typically suggested for dust (e.g., Table 1 in Schmeisser et al., 2017), however, the monthly α_a values represent all data for that month, not just during dust events which tend to be sporadic and short-lived (less than 1 to 5 days, (Hallar et al., 2015)).

Fig. 3 shows a plot of the scattering Ångström exponent (450nm/700nm) versus scattering coefficient at 550nm for PM_{10}. The scattering Ångström exponent was calculated for each hourly data point for the years 2011 – 2016. The black dots represent all data, green dots represent data collected during the peak dust season days (April 1 – May 15) at SPL (Hallar et al., 2015), and red dots represent values from the summer season defined as days (June 19 – August 13).

By comparing these two quantities, a relationship between aerosol loading and aerosol size with respect to season can be discerned. The plot shows two major aerosol categories. One group consists of small size particles and high aerosol loading located in the top portion of graph

and is associated largely with the summer months (combustion aerosols). The other is comprised of mostly coarse-mode particles (dust) on the lower portion of the plot with lower scattering that occurs mainly during the spring dust peak. Hallar et al. (2015) presented similar results; however, nephelometer and PSAP measurements in that study were limited to years 2011-2013 (2015) compared to 2011 – 2016 for this project. In Hallar et al. (2015), aerosol optical depth combined with surface level nephelometer data suggested that high altitude long-range transport may be primarily responsible for the strong dust signal observed at SPL in the spring. The expanded dataset presented here suggest otherwise, as there is a strong dust signal observed at the surface that is apparent from the decrease in in-situ scattering Ångström exponent during the spring.

The single scattering albedo for 450nm, 550nm, and 700nm wavelengths are shown in Fig. 4. SSA was highest during the spring and summer (with the exception of June) and lowest during the winter season. We hypothesize that the seasonal variability in SSA is due to the impact of wildfires in the late spring and summer, along with an increase in emissions from home heating via wood burning during the winter months (Zhao et al., 2013).

While Fig. 3 suggests that summer months are associated with wildfires, (i.e., combustion aerosol), the SSA observed during the summer is quite high. This has previously been observed for long range transport of smoke and is possibly associated with condensation of gases from wildfire smoke that can enhance the scattering of the aerosol (Andrews et al., 2004).

Though dust is observed at SPL in the spring, it is difficult to identify specific dust sources without comparison to known dust events. While infrequent, Asian dust has previously been detected at SPL though, as noted above, it was typically above the surface (Hallar et al., 2015). Hallar et al. (2015) also observed a number of dust events originating from regional (inter-mountain west) sources during the spring months. In the future, incorporation of

meteorological conditions could also yield important information regarding dust sources. Different methodologies, including aerosol chemistry, could also be utilized to identify aerosol types with higher specificity and thus help identify aerosol sources.

6 CONCLUSIONS

The identification of aerosol seasonal patterns and sources in the western U.S. is crucial for improving visibility and climate model accuracy. Here the annual cycles of aerosol optical properties (absorption, scattering, single scattering albedo. and absorption and scattering Angstrom exponents) were presented and tied to known aerosol types. A strong wildfire signal was observed in the summer at SPL, yet this was not associated with a significant decrease in SSA. The combination of these measurements suggest that the wildfire smoke is aged and processed, reducing the direct radiative forcing impact, as the smoke is transported from the initial source.

Additionally, aerosol climatology from in-situ measurements at SPL presented by Hallar et al. (2015) have been updated to include year 2013-2016. A notable new finding is the increased detection of dust by the in-situ measurements at the surface, whereas previously comparison of column and surface data suggested most of the springtime dust remained above the surface. These results point to the impacts of regional climate change on visibility with an increasingly more arid environment in the Western U.S. (Hallar et al., 2017).

Acknowledgements. Ty Atkins and Joe Messina provided technical assistance with the maintenance and data quality control for the aerosol optical instruments at SPL, and we are grateful. The Steamboat Ski Resort provided logistical support and in-kind donations. The Desert Research Institute is a permittee of the Medicine-Bow Routt National Forests and is an equal

opportunity service provider and employer. All data used in this analysis are available at: http://ebas.nilu.no

REFERENCES

Albrecht, Bruce A. (1989). Aerosols, cloud microphysics, and fractional cloudiness. *Science.* 245: 4923, 1227.

Anderson, T. L. and Ogren, J. A. (1998). Determining aerosol radiative properties using the TSI 3563 integrating nephelometer. *Aerosol Sci. Tech.* 29: 57–69.

Andrews, E., Ogren, J. A., Bonasoni, P., Marinoni, A., Cuevas, E., Rodríguez, S., Sun, J. Y., Jaffe, D. A., Fischer, E. V., Baltensperger, U., Weingartner, E., Collaud Coen, M., Sharma, S., Macdonald, A.M., Leaitch, W.R., Lin, N.H., Laj, P., Arsov, T., Kalapov, I., Jefferson, A. and Sheridan, P. (2011). Climatology of aerosol radiative properties in the free troposphere, *Atmos. Res.*, 102(4): 365-393, doi.org/10.1016/j.atmosres.2011.08.017.

Andrews, E., Sheridan, P.J., Ogren, J.A., Ferrare, R. (2004). In situ aerosol profiles over the Southern Great Plains cloud and radiation test bed site: 1. Aerosol optical properties. *J. Geophys. Res.* 109:D06208, doi:10.1029/2003JD004025.

Bergstrom, R. W., Russell, P. B., and Hignett, P. (2002). Wavelength dependence of the absorption of black carbon particles: Predictions and results from the TARFOX experiment and implications for the aerosol single scattering albedo. *J. Atmos. Sci.* 59: 567–577.

Bergstrom, R. W., Pilewskie, P., Russell, P. B., Redemann, J., Bond, T. C., Quinn, P. K., and Sierau, B. (2007). Spectral absorption properties of atmospheric aerosols. *Atmos. Chem. Phys.* 7: 5937–5943, https://doi.org/10.5194/acp-7-5937-2007

318 Bond, T. C., Anderson, T. L., and Campbell, D. (1999). Calibration and intercomparison of
319 filter-based measurements of visible light absorption by aerosols. *Aerosol Sci. Tech.* 30:
320 582–600, doi:10.1080/027868299304435
321 Charlson, R. J., Schwartz, S. E., hales, J. M., Cess, R. D., Coakley Jr., J. A., Hansen, J. E. and
322 Hofmann, D. J. (1992). Climate Forcing by Anthropogenic Aerosols. *Science.* 255: 423-
323 430, doi: 10.1126/science.255.5043.423

324 Chung, C. E., Ramanathan, V., Kim, D. and Podgorny, I.A. (2005). Global anthropogenic
325 aerosol direct forcing derived from satellite and ground-based observations. *J. Geophys.*
326 *Res.* 110: D24207, doi:10.1029/2005JD006356.
327 Clarke, A. and Kapustin, V. (2010) Hemispheric aerosol vertical profiles: Anthropogenic
328 impacts on optical depth and cloud nuclei. *Science.* 329: 1488-1492.

329 Diffenbaugh, N. S., Ashfaq, M., Shuman, B., Williams, J. W. and Bartlein, P. J. (2006). Summer
330 aridity in the United States: response to mid-Holocene changes in insolation and sea
331 surface temperature. *Geophys. Res. Lett.* 33: 22, doi.org/10.1029/2006GL028012.

332 Dubovik, O., Smirnov, A., Holben, B. N., King, M. D., Kaufman, Y. J., Eck, T. F. and Slutsker, I.
333 (2000). Accuracy assessments of aerosol optical properties retrieved from Aerosol
334 Robotic Network (AERONET) Sun and sky radiance measurements. *J. Geophys.*
335 *Res.*105(D8): 9791–9806, doi:10.1029/2000JD900040.
336 Giorgi, F.C. (2005). Climate Change Prediction. *Climatic Change*. 73: 239-265,
337 doi.org/10.1007/s10584-005-6857-4.
338 Hallar, A. G., Molotch, N. P., Hand, J. L., Livneh, B., McCubbin, I. B., Petersen, R., Michalsky,
339 J., Lowenthal, D. and Kunkel, K. E. (2017). Impacts of increasing aridity and wildfires on

aerosol loading in the intermountain Western US. *Environ. Res. Lett*. 12: 014006, doi:10.1088/1749-9326/aa510a.

Hallar, A. G., Petersen, R., Andrews, E., Michalsky, J., McCubbin, I. B. and Ogren, J. A. (2015). Contributions of dust and biomass burning to aerosols at a Colorado mountain-top site. Atmos. Chem. Phys. 15: 13665-13679, doi: 10.5194/acp-15-13665-2015.

Hallar, A. G., Petersen, R., McCubbin, I. B., Lowenthal, D., Lee, S., Andrews, E. and Yu, F. (2016). Climatology of ne particle formation and corresponding precursors at Storm Peak Laboratory. Aerosol Air Qual. Res. 16: 816-826, doi: 10/4209/aaqr.2015.05.0341.

Hand, J. L., Gill, T. E. and Schichtel, B. A. (2017). Spatial and seasonal variability in fine mineral dust and coarse aerosol mass at remote sites across the United States. *J. Geophys. Res. Atmos.* 122: 3080–3097, doi:10.1002/2016JD026290.

Haywood, J. and Boucher, O. (2000). Estimates of the direct and indirect radiative forcing due to tropospheric aerosols: A review. *Rev. Geophys*. 38: 513-543.

Hirdman, D., Sodemann, H., Eckhardt, S., Burkhart, J. F., Jefferson, A., Mefford, T., Quinn, P.K., Sharma, S., Ström, J. and Stohl, A. (2010). Source identification of short-lived air pollutants in the Arctic using statistical analysis of measurement data and particle dispersion model output. *Atmos. Chem. Phys*. 10: 669-693.

Jacobson, M. Z. (2001). Global direct radiative forcing due to multicomponent anthropogenic and natural aerosols. *J. Geophys. Res*. 106: 1551–1568. doi: 10.1029/2000JD900514.

Laj, P., Klausen, J., Bilde, M., Plaß-Duelmer, C., Pappalardo, G., Clerbaux, C., Baltensperger, U., Hjorth, J., Simpson, D., Reimann, S., Coheur, P.-F. Richter, A., De Mazière, M., Rudich, Y., McFiggans, G., Torseth, K., Wiedensohler, A., Morin, S., Schulz, M., Allan, J. D.,

Attié, J.-L., Barnes, I., Birmili, W., Cammas, J. P., Dommen, J., Dorn, H.- P., Fowler, D., Fuzzi, S., Glasius, M., Granier, C., Hermann, M., Isaksen, I.S.A., Kinne, S., Koren, I., Madonna, F., Maione, M., Massling, A., Moehler, O., Mona, L., Monks, P. S., Müller, Müller, D. T., Orphal, J., Peuch, V.-H., Stratmann, F. D., Tanré, F. and Ty G. (2009). Measuring atmospheric composition change. *Atmos. Environ.* 43: 5351–5414.

Ogren, J. A. (2010). Comment on "Calibration and Intercomparison of Filter-Based Measurements of Visible Light Absorption by Aerosols". *Aerosol Sci. Tech.* 44: 589–591, doi:10.1080/02786826.2010.482111.

Ogren, J. A., Wendell, J., Andrews, E., and Sheridan, P. J. (2017). Continuous light absorption photometer for long-term studies. *Atmos. Meas. Tech.*10: 4805-4818, http://dx.doi.org/10.5194/amt-10-4805-2017.

Pandolfi, M., Alados-Arboledas, L., Alastuey, A., Andrade, M., Angelov, C., Artiñano, B., Backman, J., Baltensperger, U., Bonasoni, P., Bukowiecki, N., Collaud Coen, M., Conil, S., Coz, E., Crenn, V., Dudoitis, V., Ealo, M., Eleftheriadis, K., Favez, O., Fetfatzis, P., Fiebig, M., Flentje, H., Ginot, P., Gysel, M., Henzing, B., Hoffer, A., Holubova Smejkalova, A., Kalapov, I., Kalivitis, N., Kouvarakis, G., Kristensson, A., Kulmala, M., Lihavainen, H., Lunder, C., Luoma, K., Lyamani, H., Marinoni, A., Mihalopoulos, N., Moerman, M., Nicolas, J., O'Dowd, C., Petäjä, T., Petit, J.-E., Pichon, J. M., Prokopciuk, N., Putaud, J.-P., Rodríguez, S., Sciare, J., Sellegri, K., Swietlicki, E., Titos, G., Tuch, T., Tunved, P., Ulevicius, V., Vaishya, A., Vana, M., Virkkula, A., Vratolis, S., Weingartner, E., Wiedensohler, A., and Laj, P. (2018). A European aerosol phenomenology – 6:

scattering properties of atmospheric aerosol particles from 28 ACTRIS sites. *Atmos. Chem. Phys.*18: 877- 7911, https://doi.org/10.5194/acp-18-7877-2018, 2018.

Raatikainen, T., Hyvärinen, A.-P. , Hatakka, J., Panwar, T.S., Hooda, R.K., Sharma, V.P. and Lihavainen, H. (2014). The effect of boundary layer dynamics on aerosol properties at the Indo-Gangetic plains and at the foothills of the Himalayas. *Atmospheric Environ.* 89: 548-555, https://doi.org/10.1016/j.atmosenv.2014.02.058.

Reddington, C. L., Carslaw, K. S., Stier, P., Schutgens, N., Coe, H., Liu, D., Allan, J. Browse, J., Pringle, K. J., Lee, L. A., Yoshioka, M., Johnson, J. S., Regayre, L.A., Spracklen, D. V., Mann, G. W., Clarke, A., Hermann, M., Henning, S., Wex, H., Kristensen, T. B., Leaitch, W.R., Pöschl, U., Rose, D., Andreae, M. O., Schmale, J., Kondo, Y., Oshima, N., Schwarz, J. P., Nenes, A., Anderson, B., Roberts, J. G., Snider, C. R., Leck, C., Quinn, P. K., Chi, X., Ding, A., Jimenez, J. L. and Zhang, Q. (2017). The Global Aerosol Synthesis and Science Project (GASSP): Measurements and Modeling to Reduce Uncertainty. *Bull. Amer. Meteor. Soc.*, 98: 1857–1877, https://doi.org/10.1175/BAMS-D-15-00317.1

Sanroma, E., Palle, E. and Sanchez-Lorenzo, A. (2010).Long-term changes in insolation and temperatures at different altitudes. *Environ. Res. Lett.* 5: 2, https://doi.org/10.1088/1748-9326/5/2/024006.

Schmeisser, L., Andrews, E., Ogren, J. A., Sheridan, P., Jefferson, A., Sharma, S., Kim, J. E., Sherman, J. P., Sorribas, M., Kalapov, I., Arsov, T., Angelov, C., Mayol-Bracero, O. L., Labuschagne, C., Kim, S. W., Hoffer, A., Lin, N. H., Chia, H. P., Bergin, M., Sun, J.,

Liu, P. and Wu, H. (2017). Classifying aerosol type using in situ surface spectral aerosol optical properties. *Atmos. Chem. Phys.* 17: 12097 – 12120.

Spracklen, D. V., Mickley, L. J., Logan, J. A., Hudman, R. C., Yevich, R., Flannigan, M. D. and Westerling, A. L. (2009). Impacts of climate change from 2000 to 2050 on wildfire activity and carbonaceous aerosol concentrations in the western United States. *J. Geophys. Res.* 114: 2156-2202, doi: 10.1029/2008JD010966.

Stocker, T. F., Qin, D., Plattner, G. K., Alexander, L. V., Allen, S. K., Bindoff, N. L., Bréon, F. M. , Church, J. A., Cubasch, U. , Emori, S., Forster, P., Friedlingstein, P., Gillett, N., Gregory, J. M., Hartmann, D. L., Jansen, E., Kirtman, B., Knutti, R., Krishna Kumar, K., Lemke, P., Marotzke, J., Masson-Delmotte, V., Meehl, G. A., Mokhov, I. I., Piao, S., Ramaswamy, V., Randall, D., Rhein, M., Rojas, M., Sabine, C., Shindell, D., Talley, L. D., Vaughan, D. G. and Xie, S. P. (2013). Technical Summary. In: *Climate Change 2013: The Physical Science Basis. Contribution of Working Group I to the Fifth Assessment Report of the Intergovernmental Panel on Climate Change* [Stocker, T.F., D. Qin, G.-K. Plattner, M. Tignor, S.K. Allen, J. Boschung, A. Nauels, Y. Xia, V. Bex and P.M. Midgley (eds.)]. Cambridge University Press, Cambridge, United Kingdom and New York, NY, USA.

Twomey, S. (1977). The Influence of Pollution on the Shortwave Albedo of Clouds. *J. Atmos. Sci.* 34: 1149–1152, doi.org/10.1175/1520-0469(1977)034<1149:TIOPOT>2.0.CO;2.

Wang, Z., French, J., Vali, G., Wechsler, P., Haimov, S., Rodi, A., Deng, M., Leon, D., Snider, J., Peng, L. and Pazmany, A.L. (2012). Single Aircraft Integration of Remote Sensing and In

Situ Sampling for the Study of Cloud Microphysics and Dynamics. *Bull. Amer. Meteor. Soc.* 93: 653-668, https: //doi.oprg/10.1175/BAMS-D-11-00044.1.

Westerling, A. L., Hidalgo, H. G., Cayan, D. R. and Swetnam, T. W. (2006). Warming and earlier spring increase western US forest wildfire activity. *Science.* 313: 940–3.

Yu, H., Remer, L. A., Chin, M., Bian, H., Kleidman, R. G., and Diehl, T. (2008): A satellite-based assessment of transpacific transport of pollution aerosol. *J. Geophys. Res.-Atmos.*113: D14S12, doi: 10.1029/2007JD009349.

Yu, H., Quinn, P.K., Feingold, G., Remer, L. A., Kahn, R.A., Chin, M., and Schwartz, S. E. (2009). Remote Sensing and In Situ Measurements of Aerosol Properties, Burdens, and Radiative Forcing, in Atmospheric Aerosol Properties and Climate Impacts, A Report by the US Climate Change Science Program and the Subcommittee on Global Change Research, edited by: Chin, M., Kahn, R.A., and Schwartz, S. E., National Aeronautics and Space Administration, Washington, D.C., US

Zhao, Y., Hallar, A.G. and Mazzoleni, L.R. (2013). Atmospheric organic matter in clouds: exact masses and molecular formula identification using ultrahigh-resolution FT-ICR mass spectrometry. *Atmos. Chem. Phys.* 13: 12343-12362, doi: 10.5194/acp-13-12343-2013.

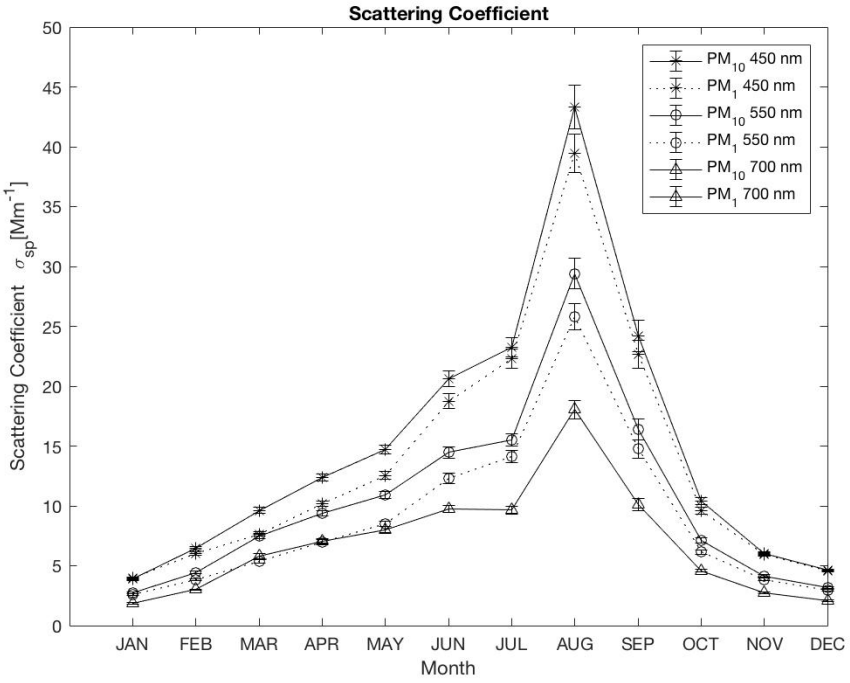

441

442 **Figure 1(a).** Mean monthly scattering coefficients for years 2011-2016. Measurements at 450, 550 and 700 nm are represented by asterisk, open
443 circle, and triangle markers, respectively. Solid lines are PM_1 and dashed lines are PM_{10}. The 95 % Confidence intervals of the monthly means are
444 displayed using error bars.

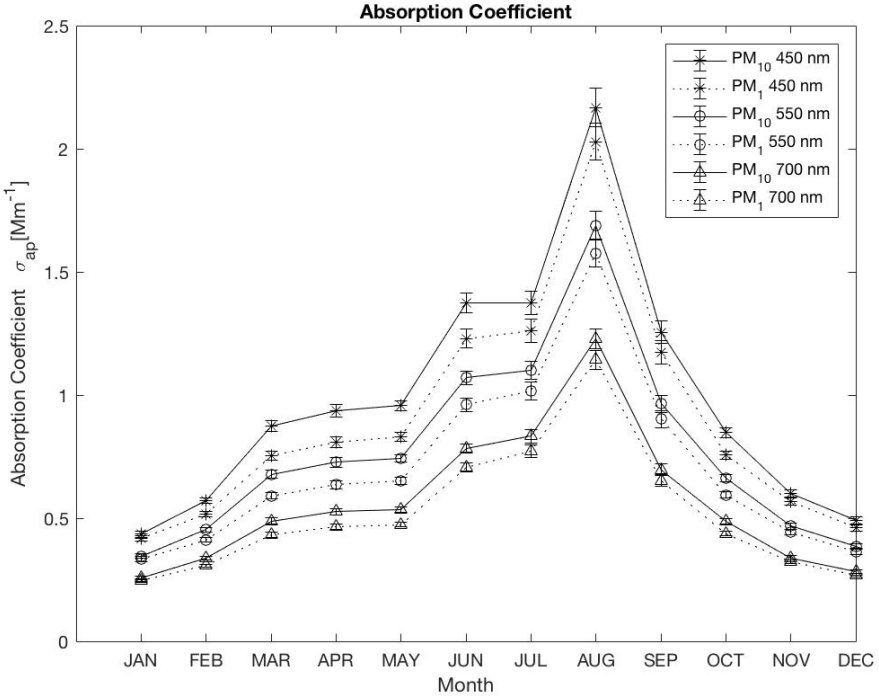

445
446
447 **Figure 1(b).** Mean monthly absorption coefficients for years 2011 – 2016. Measurements at 450 ,550 and 700 nm are represented by asterisk,
448 open circle, and triangle markers, respectively. Solid lines are PM_1 and dashed lines are PM_{10}. The 95 % Confidence intervals of the monthly
449 means are displayed using error bars.

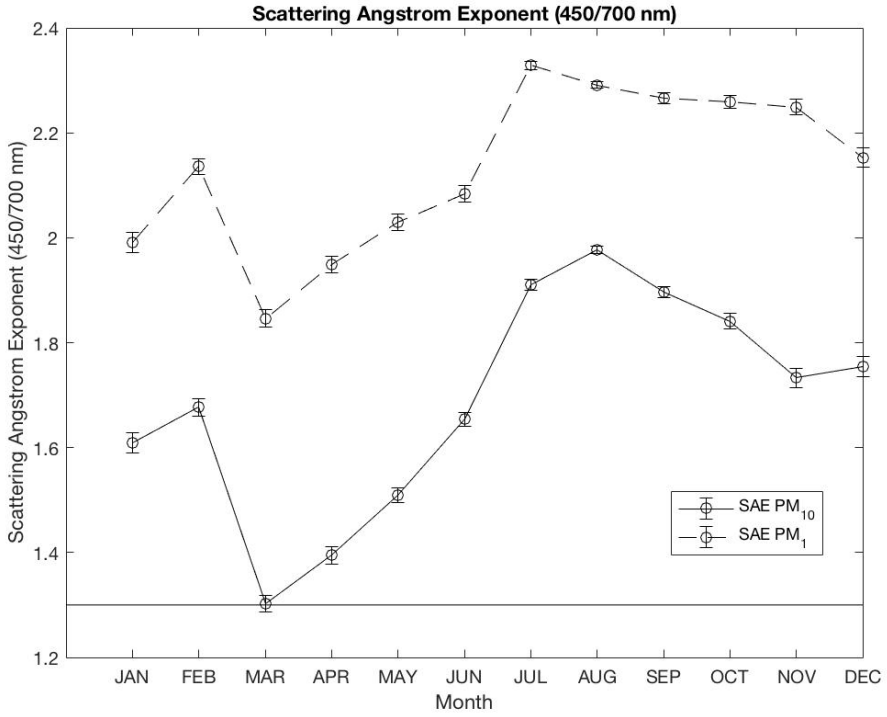

450

451 **Figure 2(a).** Mean monthly scattering Ångström exponent (400/700 nm). The sold line represents PM_{10} and dashed line PM_1. The 95 %
452 Confidence intervals of the monthly means are displayed using error bars.
453

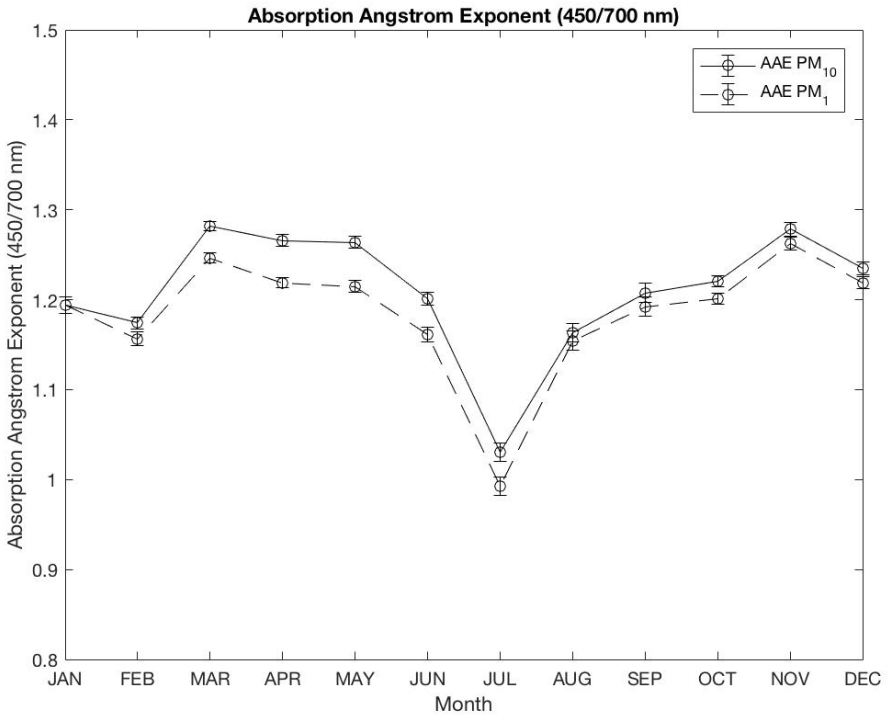

454

Figure 2(b). Mean monthly absorption Ångström exponent (400/700 nm). The sold line represents PM_{10} and dashed line PM_1. The 95 % Confidence intervals of the monthly means are displayed using error bars.

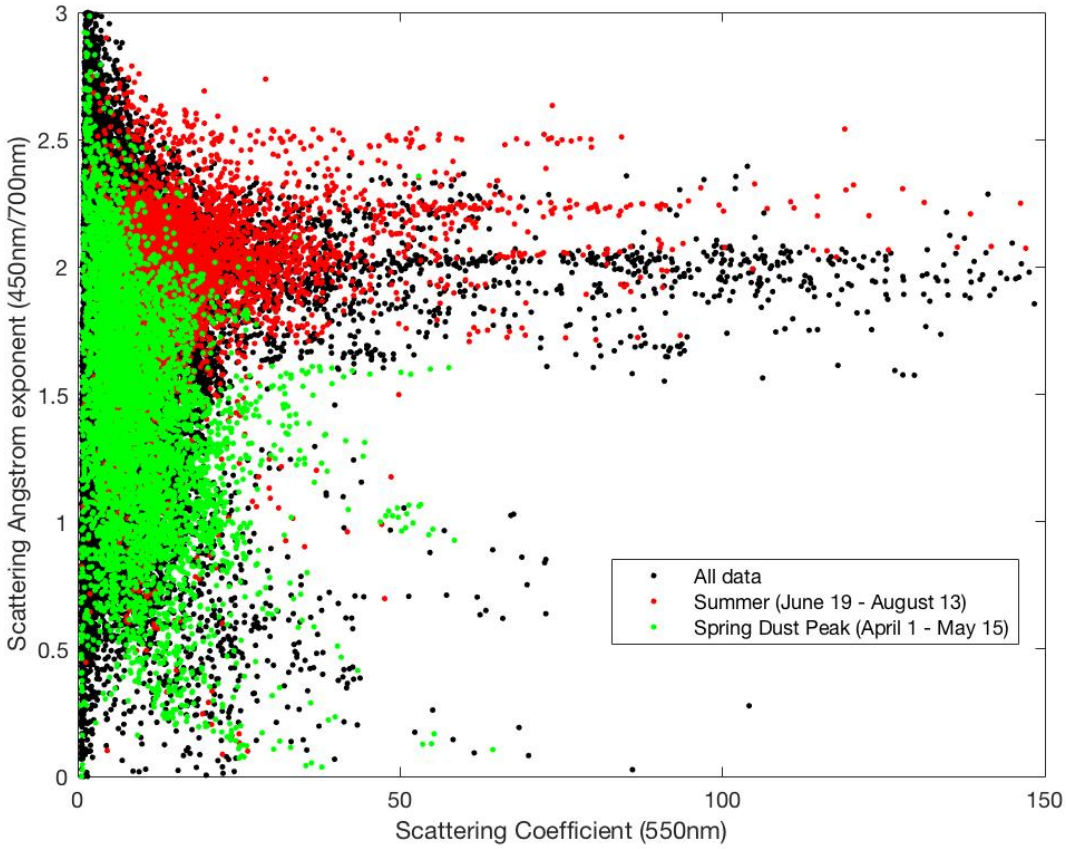

Figure 3. Ångström exponent (450/700 nm) vs. scattering coefficient at 550 nm for years 2011-2016. Black dots represent all data. Green dots occur during peak dust season (Hallar et al., 2015) from April 1 – May 15 for all years. Red dots represent summer season for days June19 – August 13 of all years.

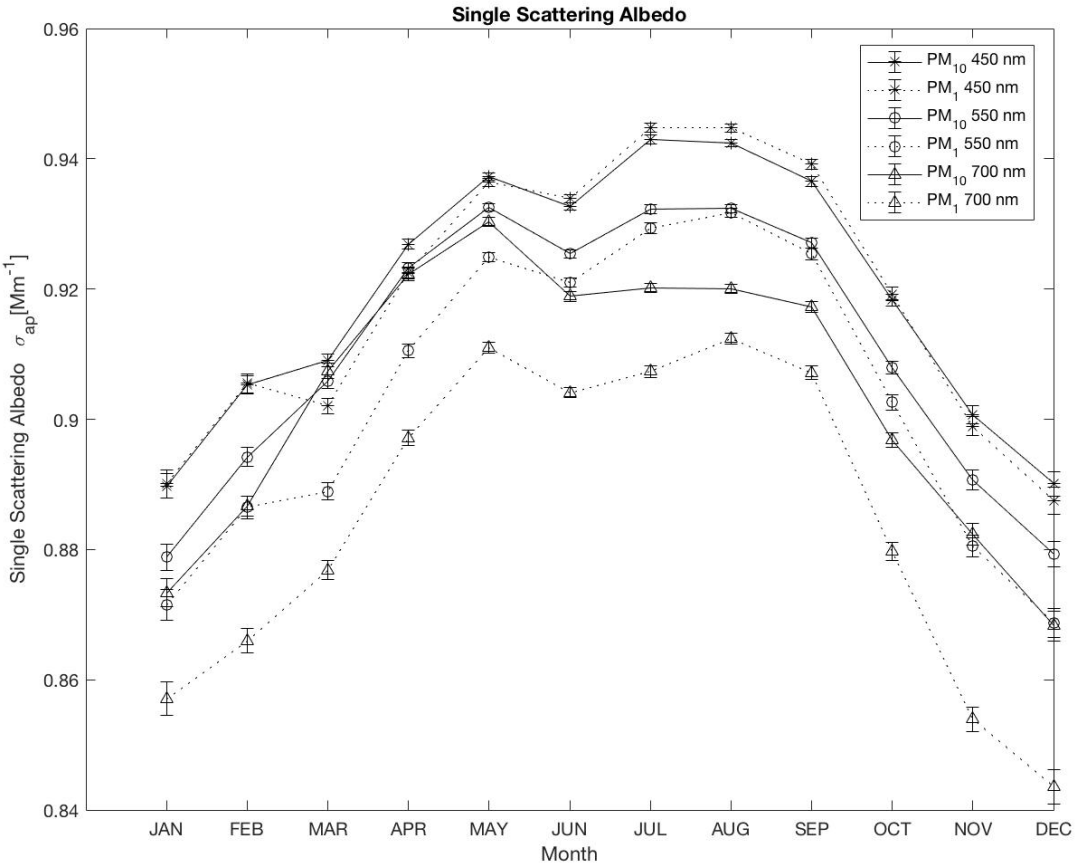

461
462 **Figure 4.** Single scattering albedo at 450 nm (asterisk), 550 nm (open circle) and 700 nm (triangle). The solid lines represent PM_{10} and the dashed
463 lines represent PM_1. The 95 % Confidence intervals of the monthly means are displayed using error bars.
464
465